

Finite gratings of many thin silver nanostrips: Optical resonances and role of periodicity

Olga V. Shapoval and Alexander I. Nosich

Citation: *AIP Advances* **3**, 042120 (2013); doi: 10.1063/1.4802880

View online: <http://dx.doi.org/10.1063/1.4802880>

View Table of Contents: <http://aipadvances.aip.org/resource/1/AAIDBI/v3/i4>

Published by the [American Institute of Physics](#).

Additional information on AIP Advances

Journal Homepage: <http://aipadvances.aip.org>

Journal Information: <http://aipadvances.aip.org/about/journal>

Top downloads: http://aipadvances.aip.org/most_downloaded

Information for Authors: <http://aipadvances.aip.org/authors>

ADVERTISEMENT



AIPAdvances

Now Indexed in Thomson Reuters Databases

Explore AIP's open access journal:

- Rapid publication
- Article-level metrics
- Post-publication rating and commenting

Finite gratings of many thin silver nanostrips: Optical resonances and role of periodicity

Olga V. Shapoval^a and Alexander I. Nosich

Laboratory of Micro and Nano Optics, Institute of Radio-Physics and Electronics NASU,
Kharkiv, 61085, Ukraine

(Received 29 January 2013; accepted 10 April 2013; published online 18 April 2013)

We study numerically the optical properties of the periodic in one dimension flat gratings made of multiple thin silver nanostrips suspended in free space. Unlike other publications, we consider the gratings that are *finite* however made of *many* strips that are *well thinner than the wavelength*. Our analysis is based on the combined use of two techniques earlier verified by us in the scattering by a single thin strip of conventional dielectric: the generalized (effective) boundary conditions (GBCs) imposed on the strip median lines and the Nystrom-type discretization of the associated singular and hyper-singular integral equations (IEs). The first point means that in the case of the metal strip thickness being only a small fraction of the free-space wavelength (typically 5 nm to 50 nm versus 300 nm to 1 μm) we can neglect the internal field and consider only the field limit values. In its turn, this enables reduction of the integration contour in the associated IEs to the strip median lines. This brings significant simplification of the scattering analysis while preserving a reasonably adequate modeling. The second point guarantees fast convergence and controlled accuracy of computations that enables us to compute the gratings consisting of hundreds of thin strips, with total size in hundreds of wavelengths. Thanks to this, in the H-polarization case we demonstrate the build-up of sharp grating resonances (a.k.a. as collective or lattice resonances) in the scattering and absorption cross-sections of sparse multi-strip gratings, in addition to better known localized surface-plasmon resonances on each strip. The grating modes, which are responsible for these resonances, have characteristic near-field patterns that are distinctively different from the plasmons as can be seen if the strip number gets larger. In the E-polarization case, no such resonances are detectable however the build-up of Rayleigh anomalies is observed, accompanied by the reduced scattering and absorption. *Copyright 2013 Author(s). All article content, except where otherwise noted, is licensed under a Creative Commons Attribution 3.0 Unported License.* [<http://dx.doi.org/10.1063/1.4802880>]

I. INTRODUCTION

Localized surface-plasmon resonances (we will call them “plasmons” for brevity) on the stand-alone and coupled noble-metal wires (in the H-polarization case) are an area of active research in nanophotonics since the 2000s,¹⁻⁴ although more recently the emphasis has been shifted to the analysis of three-dimensional plasmonic particles.⁵⁻⁸ Periodic arrays or gratings made of noble-metal nanosize elements are attracting even greater attention of research community. This is caused by the effects of extraordinarily large reflection, transmission, emission, and near-field enhancement that have been found in the scattering of light by periodic scatterers.⁹⁻¹² More broadly, these resonances display a variety of Fano shapes near so-called Rayleigh anomalies of associated infinite grating.^{10, 13, 14} Much controversy still exists around these resonances. For example, in Ref. 10 their effect was attributed to the presence of a wide dielectric substrate supporting the guided modes as

^aEmail: olga.v.shapoval@gmail.com



it was not observed for a metal-strip grating on a thin substrate. In many publications they were regarded as specific plasmons. For instance, they were called “horizontal particle plasmons” in Ref. 12 and “radiatively coupled plasmons” elsewhere, although in Refs. 10 and 15 they were reported on a metal-strip grating in the E-polarization case where no true localized surface plasmons exist at all.

It has been discovered recently, in the study of infinite gratings made of sub-wavelength dielectric or silver wires of circular cross-section suspended in free space, that these phenomena are explained by the specific poles of the field as a function of the wavelength that exist in the vicinities of Rayleigh anomalies.^{16–19} They produce the so-called grating resonances (a.k.a. collective), which should be distinguished both from the mentioned anomalies and from the plasmon resonances, whose wavelengths depend primarily on the shape and material of an individual element of the grating. In Refs. 20–22, similar poles and corresponding to them resonances have been found for infinite gratings made of thin dielectric, impedance, and silver strips, respectively.

An important question that appears in natural way is how these grating resonances develop in the more realistic case of finite gratings made of N elements. For the gratings of circular silver nanowires this has been addressed in Ref. 19 where it has been demonstrated that the grating resonances become visible if the number of elements $N \geq 10$. If it gets larger, then these resonances become sharper and approach their limit forms valid for infinite gratings.

Continuing this research, our paper deals with *finite* flat gratings made of dozens and hundreds of thin silver nanostrips. The strips are very attractive as components of optical nanoantennas and sensors due to their features like planar geometry, conformability, simplicity, and low cost of production. If manufactured with today’s technologies based on the etching and molecular-beam epitaxy, the usually have thickness between 5 and 50 nm, i.e. are well thinner than the optical wavelength. Although the first and higher-order plasmon resonances on thin strips and rods have been analyzed (see Ref. 4 and also Refs. 23–26), *periodicity-induced effects* for truly multi-element strip gratings have not been studied so far. Such analysis presents a challenging task, and our GBC-Nystrom technique operating with the small-size matrix equations offers clear advantages over the important but less economic previous methods provided that the strips are thin.

On the one hand, the finite-periodic gratings can be efficiently analyzed if the method applied to the scattering by a single element yields equations with favorable features. However usually computational cost grows up quickly and restricts the number of computable periods to a few ones like in Ref. 27 where three-groove scattering was computed.

On the other hand, the methods developed for the analysis of infinite gratings, say Refs. 9 and 10 are more economic as they exploit the periodicity by reducing the analysis to single period. However they can be inadequate if the number of strips is still in the dozens and hundreds. What is also necessary to mention, is the lack of theoretically guaranteed convergence of the methods used in many of the mentioned papers. Here we understand convergence in mathematical sense, as the possibility to reduce the error in computations to machine precision by using higher-order discretizations. Note that many non-convergent numerical techniques are still able to provide a couple of correct digits (that may frequently satisfy a need for a quick “what if?” estimation) however they fail to achieve better accuracy.

In the core of our approach lays the fact that nanostrip thickness usually makes a small fraction of the optical wavelength while the width can be both comparable to and larger than the wavelength. The small thickness suggests that the analysis can be simplified by neglecting the internal field of the strip and considering only the external field limiting values.^{28–30} This enables reduction of the integration contours in the associated IEs to the corresponding median lines at the expense of introduction of certain “effective” or generalized boundary conditions. Such an approach leads to very economic and rapidly convergent algorithms, whose results agree very well with full boundary^{2–4} and volume IE results.^{1,31,32} It has been used earlier in the analysis of the wave scattering by the *infinite* gratings of thin material strips^{20–22} using the method of analytical regularization, and more recently by a dielectric strip using the Nystrom method.³³

In this paper, we apply the Nystrom-type algorithm developed in³³ to the efficient and reliable analysis of optical effects on different objects - finite gratings of dozens and hundreds of thin silver nanostrips located in free space. Besides, we include the study of the E-polarization case where true

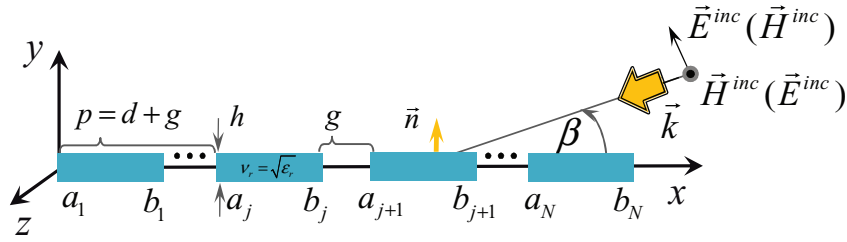


FIG. 1. Cross-sectional geometry of a finite periodic grating of N silver nanostrips infinitely long along the z -axis.

localized surface plasmon resonances are absent and the grating resonances do not contribute to the scattering and absorption because of low quality-factors. Our approach opens possibility of reliable analysis of truly multi-strip tunable optical antennas, biochemical sensors, and broadband solar-cell absorbers.

For proper positioning of our paper we would like to stress that, on the one hand, in contrast to Refs. 9–11 we consider the free-standing strip gratings. Thus the effect of the substrate is excluded and we can see what physics is associated with the silver strip grating itself. On the other hand, we consider the thin strips which do not display “vertical Fabry-Perot” (a.k.a. waveguide-mode) resonances or “vertical plasmons” observable on the thick strip metal gratings.^{11,33–36}

In the reminder of this paper, Section II presents concise summary of the formulation and method of treatment. Section III deals with numerical study of resonances in the case of H-polarization. Section IV shows comparison between finite and infinite gratings. In Section V, the case of E-polarization is presented. Conclusions are summarized in Section VI.

II. SCATTERING BY FINITE PERIODIC SILVER NANOSTRIP GRATINGS

A. Problem statement

Consider the two-dimensional scattering of the monochromatic ($\sim e^{-i\omega t}$) H-polarized electromagnetic plane wave (vector \vec{E} is across the strips) by a finite grating consisting of N parallel silver nanostrips of permittivity ϵ_r , width d , thickness h and period p (see Fig. 1). The incident wave is given as $H_z^{inc}(\vec{r}) = \exp[-ik(x \cos \beta + y \sin \beta)]$, where $\vec{r} = (x, y)$, $k = \omega/c = 2\pi/\lambda$, λ is the free-space wavelength, and the incidence angle β is measured from the x -axis.

In the presence of strips, the total field is the sum of the plane wave field and the unknown scattered field, $H_z^{sc}(\vec{r})$. The latter must satisfy the corresponding Helmholtz equation inside and outside the strips and the tangential-components continuity across strips' contours of cross-section. Besides, it must satisfy Sommerfeld radiation condition and condition of the local energy finiteness. Such a scattering problem is uniquely solvable for the function $H_z^{sc}(\vec{r})$.

B. Generalized boundary conditions

As it has been shown in Refs. 28–30, if the thickness h of a flat material slab is much smaller than the free-space wavelength λ , one can neglect the internal field inside the slab, shrink its cross-section to the median line, say S , and impose the following two-side GBCs for the external field limiting values at this line:

$$\partial H_z^+(\vec{r})/\partial \vec{n} + \partial H_z^-(\vec{r})/\partial \vec{n} = -i2kR[H_z^+(\vec{r}) - H_z^-(\vec{r})], \quad (1)$$

$$H_z^+(\vec{r}) + H_z^-(\vec{r}) = i2Qk^{-1}[\partial H_z^+(\vec{r})/\partial \vec{n} - H_z^-(\vec{r})/\partial \vec{n}]. \quad (2)$$

Here, \vec{n} is the unit vector normal to the slab top side, the indices \pm correspond to the limit values of the field at the top and bottom sides, respectively, and R and Q are the electric and magnetic resistivities, which depend on the slab refractive index $\nu_r = \epsilon_r^{1/2}$, its thickness, and the frequency. If the slab material is non-magnetic and high-contrast one, i.e. $|\epsilon_r| \gg 1$, then they are derived as

(see Ref. 30),

$$R_j = i(v_r^{-1}/2) \cot(kh v_r/2), \quad Q = i(v_r/2) \cot(kh v_r/2). \quad (3)$$

In a multi-strip configuration, we impose GBCs at $S = \cup_{j=1}^N S_j$, where $S_j = \{(x, 0) : x \in [a_j, b_j]\}$, and a_j and b_j are the strips endpoints. As certified by the data of Ref. 37, the mentioned assumption is valid in the visible range from 400 nm to 900 nm for the nanostrips made of silver or gold. This is not completely so between 300 nm and 400 nm and the results computed in that range may need further validation that will be presented elsewhere. According to the earlier studies (see Ref. 32), the strip thickness should be larger than 2 nm: if the strip is thinner, one has to replace the classical bulk refractive index model with a quantum-chemistry or jellium model.

Substitution of the cross-section contour or domain with the median line simplifies considerably the numerical analysis. This is because it leads to the IEs where the integration is done along a finite open interval and the unknowns are effective electric and magnetic currents. Their edge behavior can be taken into account analytically and hence there is no need for denser meshing the vicinities of the contour corners. Note that previously developed algorithms based on the volume IEs,^{1,31,32} where the integration domain is the area of the strip cross-section, have led to the numbers of unknowns in thousands, even for a stand-alone strip and apparently “graphical” accuracy of 2-3 digits. The boundary IEs²⁻⁴ are considered more efficient as they imply the discretization of the boundary instead of the area; still typical number of unknowns is in hundreds. More essentially, boundary IEs can be cast, unlike volume IEs, to the forms having non-singular and integrable kernels and thus can be discretized more reliably. In contrast, proposed median-line IEs lead to the matrices that are only slightly larger than the size of the median line in the delocalized surface-plasmon wave lengths (i.e. in small dozens for one strip) for the guaranteed 4-digit accuracy in the surface-current computations.³³

C. Singular and hyper-singular integral equations

To find the scattered magnetic field, we use the potential theory and seek this function as a sum of $2N$ terms satisfying both Helmholtz equation and the radiation condition,

$$H_z^{sc}(\vec{r}) = \sum_{j=1}^N \left[k \int_{S_j} v_j(\vec{r}') G(\vec{r}, \vec{r}') d\vec{r}' + \int_{S_j} w_j(\vec{r}') \frac{\partial G(\vec{r}, \vec{r}')}{\partial \vec{n}(\vec{r}')} d\vec{r}' \right], \quad (4)$$

where $G(\vec{r}, \vec{r}') = (i/4)H_0^{(1)}(k|\vec{r} - \vec{r}'|)$ is the free-space Green function, and the unknowns are effective electric $v_j(\vec{r}) = ik[H_z^+(\vec{r}) - H_z^-(\vec{r})]$ and magnetic $w_j(\vec{r}) = ik^{-1}[\partial H_z^+(\vec{r})/\partial \vec{n} - H_z^-(\vec{r})/\partial \vec{n}]$ currents, respectively.

As it was discussed in Ref. 33, substitution of (4) into GBC reduces the formulated scattering problem to two independent sets of coupled IEs, each of the size N . One of them contains logarithmically singular equations, and the other - hyper-singular equations,

$$4Qv_i(x_0^i) + k \sum_{j=1}^N \int_{a_j}^{b_j} v_j(x^j) H_0^{(1)}(k|x^j - x_0^i|) dx = 4ie^{-ikx_0^i \cos \beta}, \quad x_0^i \in S_i, \quad i = 1, \dots, N, \quad (5)$$

$$4Rw_i(x_0^i) + \sum_{j=1}^N \int_{a_j}^{b_j} w_j(x^j) \frac{H_1^{(1)}(k|x^j - x_0^i|)}{|x^j - x_0^i|} dx = 4 \sin \beta e^{-ikx_0^i \cos \beta}, \quad x_0^i \in S_i, \quad i = 1, \dots, N, \quad (6)$$

where integral terms in (6) are understood in the sense of finite part of Hadamard.

D. Nystrom-type numerical model

To solve IE (5), we use the Nystrom-type discretization based on the Gauss-Legendre quadrature formulas (QF). In IE (6), we at first introduce new unknown regular function $\tilde{w}_j(x^j)$: $w_j(x^j) = \tilde{w}_j(x^j)(x^j - a_j)^{1/2}(b_j - x^j)^{1/2}$, $x^j \in [a_j, b_j]$ and then apply weighted QF (with Chebyshev weight) of interpolation type with the nodes at zeros of the Chebyshev polynomials of the 2-nd kind. The mathematical details can be found in Ref. 33). As discussed there, such a combination of the material strip model based on the GBC (1) and the Nystrom-type algorithm of IE discretization has mathematically guaranteed convergence (at least as $1/n$ where n is the order of interpolation polynomial) and leads to efficient and economic numerical solution having easily controlled accuracy of computations.

E. Optical response characteristics

Using the large-argument asymptotics for the Hankel functions in the kernels of (4), the scattered magnetic field in the far zone can be represented as $H_z^{sc} \sim (2/i\pi kr)^{1/2} e^{ikr} \Phi(\varphi)$, where $\Phi(\varphi)$ is the far-field scattering pattern (or scattering diagram). It is found as

$$\Phi(\varphi) = (ik/4) \sum_{j=1}^N \int_{S_j} [v_j(x) - i \sin \varphi w_j(x)] e^{-ikx \cos \varphi} dx. \quad (7)$$

For a finite grating, the figures-of-merit are not the reflectance, transmittance and absorbance introduced in the infinite-grating scattering but the total scattering cross section (TSCS) and the absorption cross-section (ASC). These quantities are determined as follows:

$$\sigma_{sc} = (2/\pi k) \int_0^{2\pi} |\Phi(\varphi)|^2 d\varphi, \quad (8)$$

$$\sigma_{abs} = \sum_{j=1}^N \int_{S_j} [\text{Re } Q |v_j(x)|^2 + \text{Re } R |w_j(x)|^2] dx. \quad (9)$$

The sum of (8) and (9) is the extinction cross-section, and the optical theorem tells that $\sigma_{sc} + \sigma_{abs} = -(4/k) \text{Re} \Phi(\beta + \pi)$. In our computations, this relation has been always fulfilled with accuracy close to machine precision.

III. H-POLARIZATION: SURFACE PLASMON RESONANCES AND GRATING RESONANCES

In our previous papers,³³ we have computed the plasmon effects on the stand-alone silver and gold nanostrips of small thickness (e.g., $h = 5$ or 10 nm), and their periodic ensembles consisting of only several strips. As it is shown below, more massive finite nanostrip gratings, both in terms of each strip size and their number, demonstrate new features induced by their periodicity. Note that GBC (1)-(3) do not imply that the H-field is constant inside the strip as the arguments of the R and Q functions can be arbitrary.³⁰ To characterize the complex dielectric permittivity of silver we took the experimental data of Ref. 37 and used an Akima spline interpolation.

For the sake of comparison, in Fig. 2 we present the wavelength scans of the normalized by $2d$ values of TSCS and ACS for a stand-alone silver strip of the width $d = 150$ nm for three different values of strip thickness, $h = 10, 20$ and 50 nm (dotted curves).

Here, an H-polarized plane wave is incident at the strip from the normal direction. The surface plasmon resonances (marked with stars) are visible at $\lambda_1^P = 629$ nm, 515 nm and 431 nm, respectively, i.e. thinner strips have plasmon resonances red-shifted relatively to the thickest strip of $h = 50$ nm. These are Fabry-Perot-like resonances of the order 1 corresponding to the strip width equal approximately to half-wavelength of the short-range surface-plasmon wave of the corresponding silver layer.⁴

In the violet range, thinner strips have additional resonances on the higher-order plasmon resonances of the index 3 that are better visible on the ACS plots. Note that similar third-order resonances on metal nanobelts have been observed in Ref. 13.

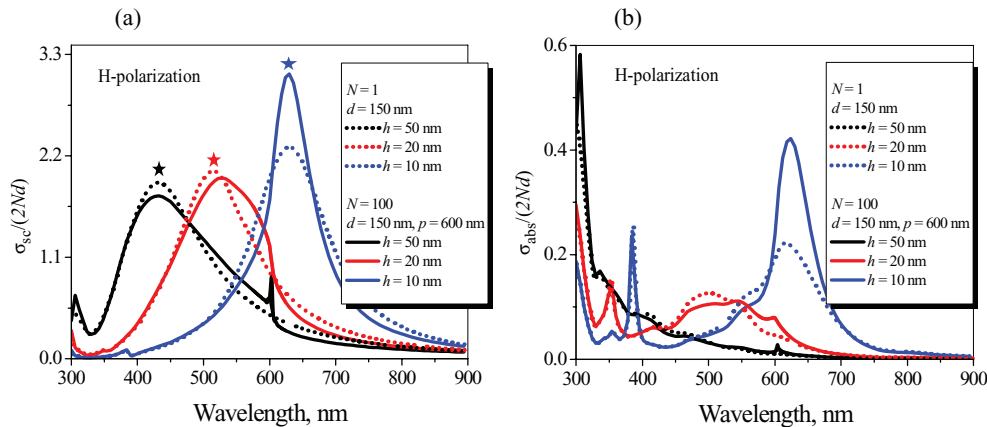


FIG. 2. Normalized TSCS (a) and ACS (b) per one strip versus the wavelength for $N = 1$ (dotted curves) and $N = 100$ (solid curves) silver strips of width $d = 150$ nm and $p = 600$ nm for three values of thickness $h = 10, 20$ and 50 nm at the normal incidence ($\beta = \pi/2$) of the H-polarized plane wave.

Besides, in Fig. 2 presented are the normalized by $2Nd$ values of TSCS and ACS plotted as a function of the wavelength for $N = 100$ silver strips of the same width and the same three thickness values, assembled in the grating with period $p = 600$ nm (solid curves).

As one can observe, the surface-plasmon resonances on the gratings have almost the same wavelengths of 630 nm, 528 nm and 432 nm, respectively, as on a stand-alone strip. However, the periodicity of the grating of 100 strips leads to the other type of resonance phenomena, so-called grating resonances.^{16–22} The thickest-strip grating (50 nm, black curves) demonstrates two grating-type resonances in the visible range, at $\lambda_1^G = 603$ nm (slightly larger than p) and $\lambda_2^G = 305$ nm (slightly larger than $p/2$). Note that the strip thickness plays important role: if strips are thin as 10 or even 20 nm, the grating resonances have almost no effect on TSCS and ACS (this effect appears if $N \gg 100$). Therefore, to obtain complete picture of the periodicity-induced effects, our further analysis will be concentrated on the study of the finite gratings made of silver strips of 50 -nm thickness.

Consider now finite gratings made of $N = 10, 20, 50$ and 200 silver strips with the width $d = 300$ nm, thickness $h = 50$ nm and period $p = 800$ nm, illuminated by a normally incident plane H-wave (see Fig. 3, solid curves). For comparison, the data for the single-strip scattering are also shown.

As follows from the stand-alone silver strip TSCS and ACS behavior (black curves), there are two plasmon resonances at $\lambda_1^P = 680.45$ nm and $\lambda_3^P = 354.1$ nm, of the first and third orders, respectively. The corresponding near and far field patterns are presented in Fig. 4; they resemble similar resonance patterns on metal nanobelts.¹³

If N similar strips are collected into a finite flat grating with period of 800 nm, they keep the plasmon resonances almost intact however additionally demonstrate the build-up of two grating resonances in the visible range: slightly above the wavelength value equal to period and slightly above the twice smaller value (colored curves in Fig. 3). These resonances become more intensive and narrower with increasing N . Here, the resonance at $\lambda_1^G = 802.6$ nm has a classical lorentzian shape, while the other resonance at $\lambda_2^G = 402$ nm displays a more complicated Fano shape as shown in the corresponding inset. This agrees well with observations of Fano resonances on other gratings – see review¹⁴ for references.

It is interesting to visualize the near-field patterns emerging at the resonance wavelengths because each of them, in the vicinity of the grating, is close to the field of the corresponding natural mode of the grating as a periodic open resonator.^{18,19,22} In Figs. 5 and 6, presented are the total magnetic near-field patterns for the 200 -strip grating with period $p = 800$ nm at the plasmon resonance wavelengths $\lambda_1^P = 680.45$ nm (a), $\lambda_3^P = 354$ nm (b) and the grating resonance wavelengths $\lambda_1^G = 802.6$ nm (a), $\lambda_2^G = 402$ nm (b), respectively.

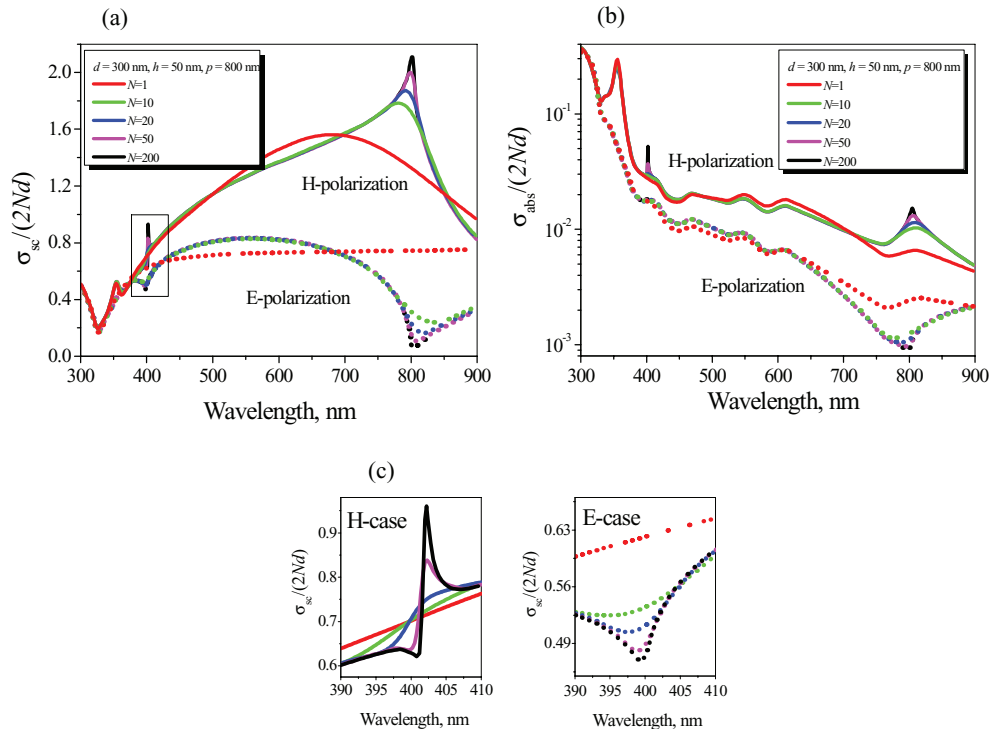


FIG. 3. Normalized TSCS (a) and ACS (b) per one strip as a function of the wavelength for $N = 1, 10, 20$ and 50 silver strips of the width $d = 300$ nm, thickness $h = 50$ nm and period $p = 800$ nm at the normal incidence of the H-wave (solid curves) and E-wave (dotted curves). Panel (c) shows zoomed TSCS near the grating resonances $\lambda = \pi/2$ in H-case and E-case, respectively.

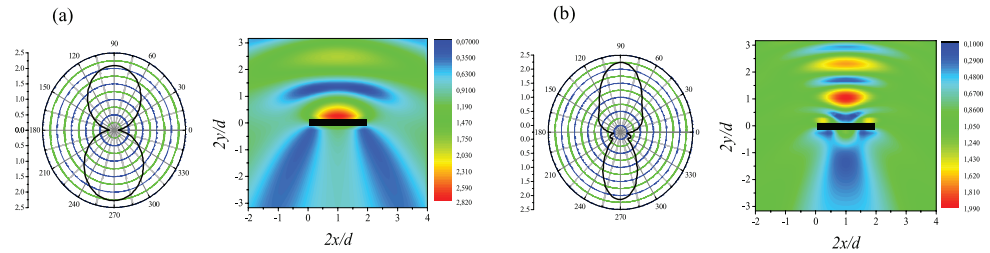


FIG. 4. H-polarization: Scattered far-field and total near field patterns for a stand-alone silver strip (black curve) at the first (a) and third (b) order surface plasmon resonances on $\lambda_1^P = 680.45$ nm and $\lambda_3^P = 354.1$ nm, respectively.

As visible in Figs. 5(a) and 5(b), in the plasmon resonances each strip supports characteristic field pattern very similar to the stand-alone strip pattern of the corresponding panel in Fig. 4. These patterns have the hot spots sticking to the strip surface and corresponding, in number, to the half-waves of the delocalized surface-plasmon standing wave excited on each strip. Behind each strip, there is a deep shadow.

From the analysis of wave scattering by infinite gratings of wires^{18,19} and strips²² it is known that in the grating resonance near the $\pm m$ -th Rayleigh anomaly the other standing wave appears in the near field, built from two Floquet spatial harmonics of the orders $\pm m$. The latter standing wave occupies a band of space along the grating and has a characteristic pattern: its hot spots are $2m$ per period independently of the strip dimensions and stretch to the distance of several periods, in the normal direction. In the patterns of Figs. 6(a) and 6(b), one can observe such standing waves along the x -axis which have $m = 1, 2$ and maximum magnitudes of 6.8 and 5.88, respectively. Note that

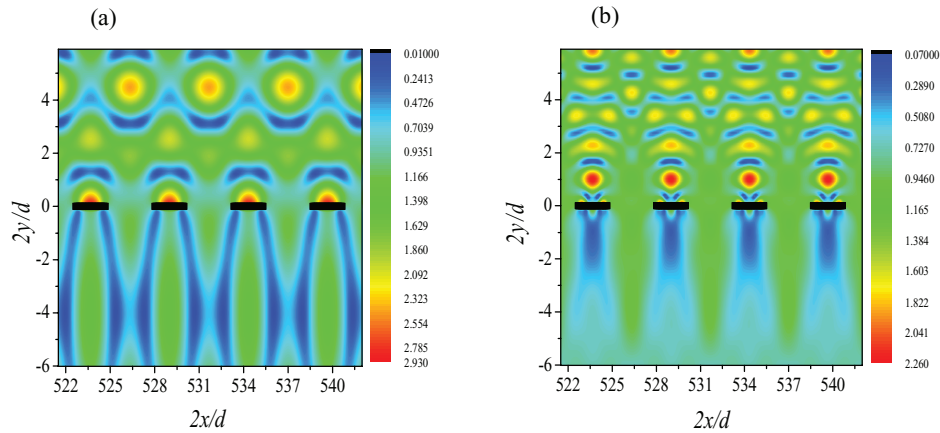


FIG. 5. Near H-field patterns around strips ## 99 to 102 for the H-wave normally incident at the grating of $N = 200$ silver strips of $d = 300$ nm, $h = 50$ nm and $p = 800$ nm for the first and third order plasmon resonances at $\lambda_3^P = 680.45$ (a) and $\lambda_3^P = 354$ (b) nm and, respectively.

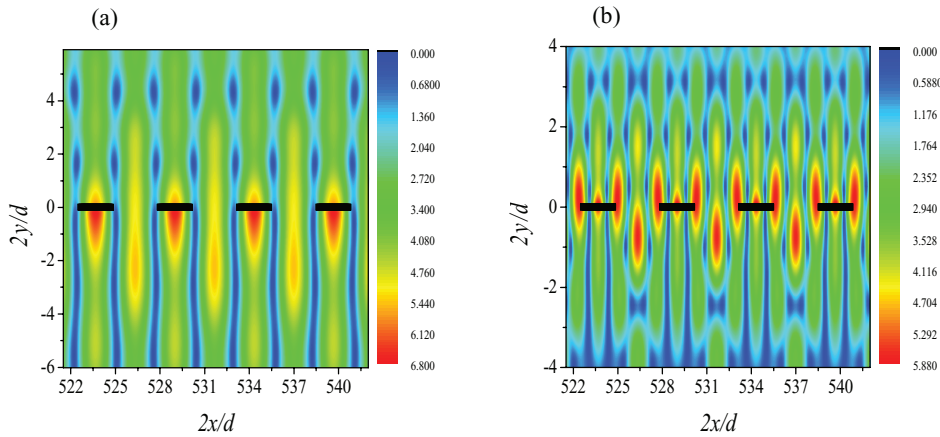


FIG. 6. Near H-field patterns around strips ## 99 to 102 for the H-wave normally incident at the grating of $N = 200$ silver strips of $d = 300$ nm, $h = 50$ nm and $p = 800$ nm for the grating resonances at $\lambda_1^G = 802.6$ nm (a) and $\lambda_2^G = 402$ nm (b).

these standing waves are not visible well in the case of smaller number of strips, e.g. $N = 20$ or 50 , or thinner strips, e.g. with $h = 10$ nm.

IV. COMPARISON BETWEEN FINITE AND INFINITE GRATINGS FOR THE H-WAVE SCATTERING

It is interesting to compare the optical properties of finite and infinite silver strip gratings, provided that a common figure-of-merit has been selected. This is not an obvious matter. However, we have found that the reflectance of a plane wave by a *finite* grating can be introduced as the part of TSCS associated with the power scattered into the upper half-space. The transmittance of finite grating can be introduced in similar manner however with account of the optical theorem. In addition, we normalize these values by the total electric width of the grating Nkp that yields,

$$R_{fin} = 2/(\pi Nkp) \int_0^\pi |\Phi(\varphi)|^2 d\varphi, \quad (10)$$

$$T_{fin} = 1 + \frac{2}{\pi Nkp} \int_\pi^{2\pi} |\Phi(\varphi)|^2 d\varphi + \frac{4}{Nkp} \text{Re}\Phi(\varphi + \beta), \quad (11)$$

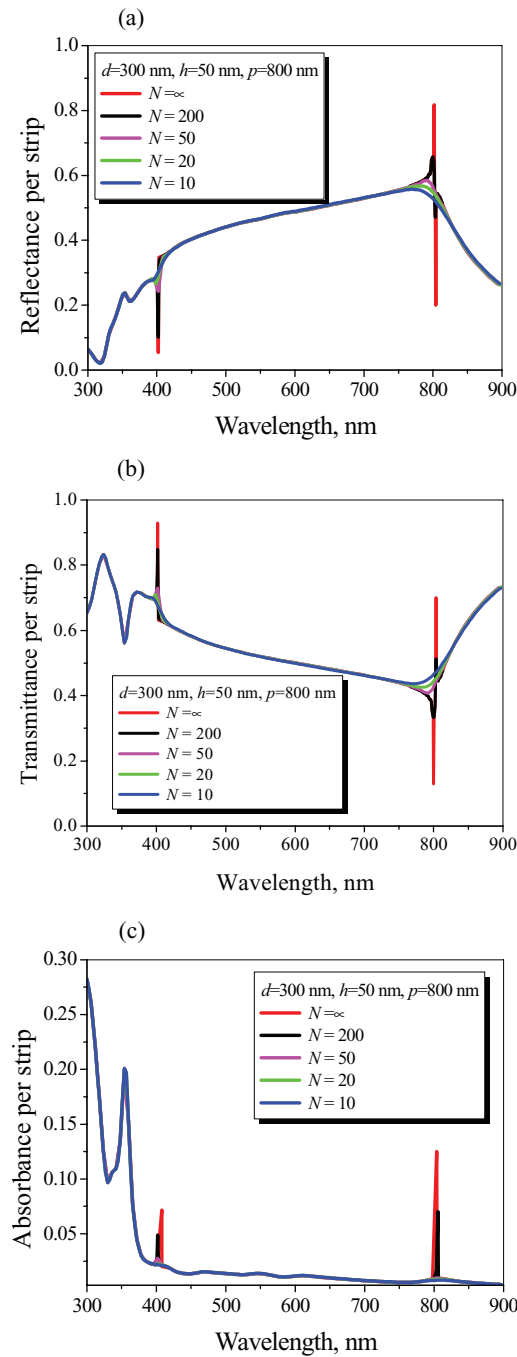


FIG. 7. Reflectance (a), transmittance (b) and absorbance (c) per one strip for the normally incident plane H-wave scattered by the infinite and $N = 10, 20, 50, 200$ strip gratings of $d = 300$ nm, $h = 50$ nm and $p = 800$ nm.

Then it is easy to see that, similarly to the infinite grating case, $|T|, |R| \leq 1$ and the absorbance can be found as $A_{fin} = 1 - (T_{fin} + R_{fin})$ that follows from the conservation of power. Interestingly, the first and the third terms in (11) cancel each other when $N \rightarrow \infty$.

These quantities can be conveniently compared to the reflectance, transmittance and absorbance of infinite grating, respectively. In Fig. 7, we present such comparison for the H-wave scattering by finite ($N = 10, 20, 50$ and 200) and infinite strip gratings of $d = 300$ nm, $h = 50$ nm and $p = 800$ nm, at the normal incidence. Note that a 200-strip grating presents, in this range, a scatterer whose total

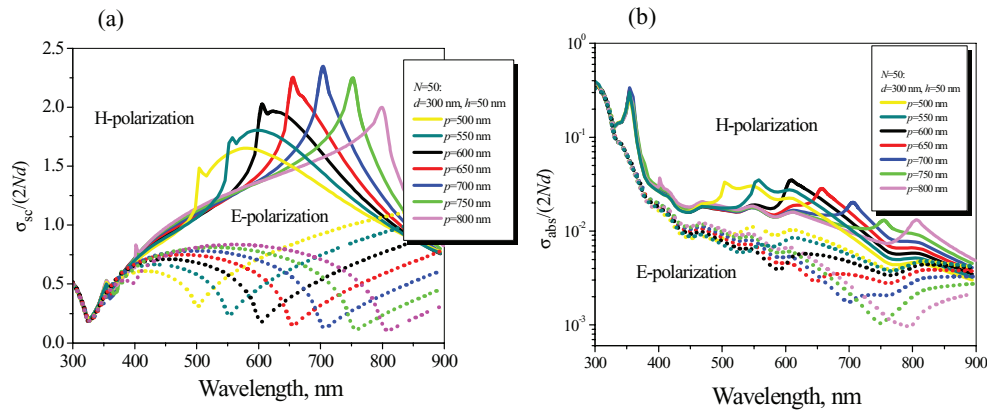


FIG. 8. Normalized TSCS (a) and ACS (b) per one strip versus the wavelength for the normally incident ($\beta = \pi/2$) H-wave (solid curves) and E-wave (dotted curves) scattering by $N = 50$ silver strip grating of $d = 300$ nm and $h = 50$ nm in dependence of the period.

size is from 180λ to 500λ . Computing such a scatterer by any of the earlier algorithms of Refs. 1–4 or any commercial software is completely out of question.

To compute the scattering by infinite strip grating, we have used the same Nystrom algorithm with the Hankel function replaced, in the kernels of IEs, with the pseudo-periodic Green's function having the phase factor of $\exp(ikp \cos \beta)$ as dictated by the incident wave.

As visible, even for 20 strips the introduced above reflectance, transmittance and absorbance values are very close to the infinite-grating values at all wavelengths from 300 nm to 900 nm, except for the narrow bands around the grating resonances just above $\lambda \approx p$ and $\lambda \approx p/2$.

The shape of the grating resonance depends on the number of periods and the studied quantity.

If, the 50-nm thick strips demonstrate sharp resonances of Fano shape on the reflectance and transmittance curves (Fig. 7(a) and 7(b)), and a Lorentz shape on the absorbance curve. This difference is explained by the interference between the incident and the scattered field parts that does not influence the absorption inside the strip. For the same geometry, the TSCS curves (Fig. 3(a) and 3(b)) display only a Lorentzian-shape resonance above $\lambda \approx p$ however again a Fano-shape above $\lambda \approx p/2$ where more than one quasi-Floquet harmonic contributes to the scattering.

Another interesting question is the optimal grating parameters for observing the most pronounced resonances. We have computed the normalized TSCS as a function of the wavelength for the $N = 50$ silver-strip gratings with several different periods (Fig. 8).

Here, plasmon resonances are near their stand-alone strip values while the grating resonances shift with period.

As one can see from this figure (from yellow to black curves), if the period of the grating is smaller than the first-order strip-plasmon wavelength of 680 nm, the grating resonance demonstrates a Fano-shape response in TSCS. If it is larger than that value, the grating resonance turns to more conventional Lorentzian shape, apparently because of less intensive optical interactions between the strips. For the considered here grating of 300×50 nm² strips, the most pronounced grating resonance has been found for the period $p = 700$ nm (blue curve) when it overlaps with the first plasmon resonance of the strip. In-resonance strip apparently scatters as a larger obstacle and, as a consequence, the build-up of the grating resonance is more efficient. Besides, in this case the merging of the third-order plasmon and the second-order grating resonance occurs around 355 nm.

V. E-POLARIZATION: SCATTERING SUPPRESSION AT RAYLEIGH ANOMALIES

In the alternative case of the E-polarized plane wave scattering (vector \vec{E} is parallel to the strips), we look for the unknown field function that is the only non-zero component of the electric field, $E_z^{sc}(\vec{r})$. Here, the GBCs (1)-(2) are also valid provided that H_z is replaced with E_z and R and Q exchange places.

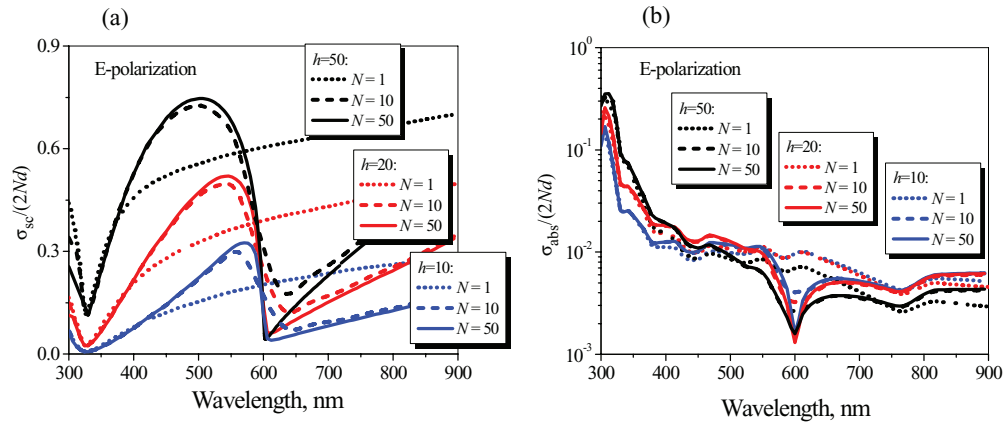


FIG. 9. Normalized TSCS (A) and ACS (B) per one strip versus the wavelength for $N = 1, 10$ and 50 silver strips of width $d = 150$ nm and $p = 600$ nm in dependence of the thickness $h = 10$ nm (blue curves), 20 nm (red) and 50 nm (black) under a normally incident E-wave ($\beta = \pi/2$).

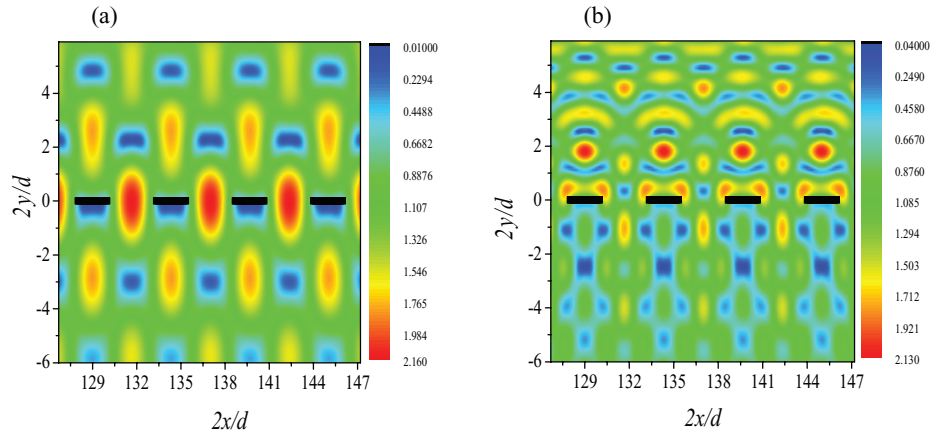


FIG. 10. Near E-field patterns around the strips ## 9 to 12 for the E-wave normally incident at the grating of $N = 50$ silver strips of $d = 300$ nm, $h = 50$ nm and $p = 800$ nm at the Rayleigh anomalies wavelengths $\lambda_1^R = 806.8$ nm (a) and $\lambda_2^R = 399.4$ nm (b).

As a result of such duality, the E-polarization case reduces to two IEs like (5) and (6) however with R and Q exchanging their places. Although this difference may seem small, it entails major modifications in the behavior of the components of extinction cross sections.

This can be observed from the comparison of the curves in Fig. 9 and Fig. 2 where the scans of TSCS and ASC are shown for the strips of three different values of thickness.

Additionally, the E-polarization spectra are shown in Figs. 3 and 8 as dotted curves. As one can see, on the silver-strip grating the E-polarized wave does not produce any noticeable response that can be interpreted as the grating resonances. This is because the associated Q-factors are much smaller in the E-case than in the H-case (by a factor $|\epsilon_r|^{-2}$), as it has been found in the analytical study of infinite strip grating.²²

Instead, one can see a gradual build-up of the Rayleigh anomalies as the strip number gets larger; this takes form of suppression of both the scattering and the absorption at the wavelengths that quickly tend (at $N > 20$) to the exact values of the associated Rayleigh wavelengths, $\lambda_m^R = p/m$, $m = 1, 2$. As can be found, this is because here the strips happen to be located in the deep minima of the electric field. Indeed, investigation of the E-field in the dips of TSCS, namely at $\lambda_1^R = 806.8$ nm and $\lambda_2^R = 399.4$ nm for an $N = 50$ strip grating with parameters $d = 300$ nm, $h = 50$ nm and $p = 800$ nm (see Fig. 10) demonstrates the $|E_z|$ minima at the strips and low-intensity maxima between them.

In the case of inclined incidence, the revealed above features of the H and E-wave scattering by finite strip gratings become more complicated as the Rayleigh anomalies split into pairs and associated grating resonances take place near each of the corresponding wavelengths. Besides, at the inclined incidence the plane H-wave excites the strip surface plasmon resonances of the even orders in addition to odd orders, presented above.

VI. CONCLUSIONS

Summarizing, we have presented accurate numerical analysis of the resonance phenomena caused by the periodicity in the scattering and absorption of the H- and E-polarized light by free-standing sparse finite flat gratings of large number of thin silver nanostrips. Our modelling has been based on the elimination of the internal fields inside strip grating with the aid of generalized boundary conditions imposed on the strip median lines. Such a simplification leads to two independent sets of N coupled integral equations, one log-singular and the other hyper-singular. For the building of the discrete model we have used the developed earlier Nystrom-type method based on the quadrature formulas of interpolation type. The resulting algorithm is efficient and reliable, with guaranteed convergence and controlled accuracy of computations.

We have demonstrated two different types of resonances in the scattering and absorption of the H-polarized light: the surface plasmon resonances on the strips and the grating resonances induced by the periodicity. We have studied how they depend on the dimensions and the number of silver nanostrips in the finite grating. The surface-plasmon resonances keep almost the same wavelength and shape as for a stand-alone silver strip regardless the strip number. In contrast, if this number grows and reaches several dozens or hundreds, quite sharp peaks associated with the grating-type resonances appear at the wavelengths slightly larger than the Rayleigh anomalies of associated infinite grating (that is $\lambda_m^R = p/m$, $m = 1, 2, \dots$ at the normal incidence). Thus, the grating resonances show little dispersion however are still sensitive to the silver strip dimensions in the sense that the shorter gratings of more massive strips demonstrate more pronounced resonances. In the case of the E-polarized light, the same gratings do not possess surface-plasmon resonances and do not show any noticeable response at the grating resonances however demonstrate the formation of the Rayleigh anomalies if the strip number gets larger. Note that, being restricted with paper length, we have focused our numerical analysis on the sparse strip gratings having the slot width comparable or larger than the strip width. The properties of dense gratings, i.e. those having narrow slots, are also interesting because of enhanced transmission in the resonances however require a separate publication.

ACKNOWLEDGMENTS

The authors are grateful to D.M. Natarov, R. Sauleau and J. Zyss for many fruitful discussions. This work was supported in part by the National Academy of Sciences of Ukraine via the State Target Program “Nanotechnologies and Nanomaterials” and the European Science Foundation via the Research and Networking Programmes “Plasmon-Nanobiosense” and “Newfocus.”

- ¹J. P. Kottmann and O. J. F. Martin, “Plasmon resonant coupling in metallic nanowires,” *Optics Express* **8**(12), 655–663 (2001).
- ²J.-W. Liaw, “New surface integral equations for the light scattering of multi-metallic nanoscatterers,” *Eng. Analysis Boundary Methods* **31**, 299–310 (2007).
- ³V. Giannini and J. A. Sánchez-Gil, “Calculations of light scattering from isolated and interacting metallic nanowires of arbitrary cross section by means of Green’s theorem surface integral equations in parametric form,” *J. Opt. Soc. Am. A* **24**(9), 2822–2830 (2007).
- ⁴T. Søndergaard and S. I. Bozhevolnyi, “Strip and gap plasmon polariton optical resonators,” *Phys. Stat. Sol. (b)* **245**(1), 9–19 (2008).
- ⁵V. Myroshnychenko, E. Carbó-Argibay, I. Pastoriza-Santos, J. Pérez-Juste, L. M. Liz-Marzán, and F. J. García de Abajo, “Modeling the optical response of highly faceted metal nanoparticles with a fully 3D boundary element method,” *Adv Mat* **20**, 4288 (2008).
- ⁶A. M. Kern and O. J. F. Martin “Surface integral formulation for 3D simulations of plasmonic and high permittivity nanostructures,” *J. Opt. Soc. Am. A* **26**(4), 732–740 (2009).

- ⁷J. M. Taboada, J. Rivero, F. Obelleiro, M. G. Araújo, and L. Landesa, "Method-of-moments formulation for the analysis of plasmonic nano-optical antennas," *J. Opt. Soc. Am. A* **28**(7), 1341–1348 (2011).
- ⁸R. Rodríguez-Oliveros and J. A. Sánchez-Gil "Localized surface-plasmon resonances on single and coupled nanoparticles through surface integral equations for flexible surfaces," *Opt Express* **19**(13), 12208–19 (2011).
- ⁹G. Schider, J. R. Krenn, W. Gotschy, B. Lambrecht, H. Ditlbacher, A. Leitner, and R. F. Aussenegg, "Optical properties of Ag and Au nanowire gratings," *J. Appl. Phys.* **90**(8), 3825–3830 (2001).
- ¹⁰A. Christ, T. Zentgraf, J. Kuhl, S. G. Tikhodeev, N. A. Gippius, and H. Giessen, "Optical properties of planar metallic photonic crystal structures: experiment and theory," *Phys. Rev. B* **70**(12), 125113–15 (2004).
- ¹¹M. R. Gadsdon, I. R. Hooper, and J. R. Sambles, "Optical resonances on sub-wavelength lamellar gratings," *Opt. Exp.* **16**(26), 22003–22028 (2008).
- ¹²A. Mendoza-Suárez, F. Villa-Villa, and J. A. Gaspar-Armenta, "Numerical method based on the solution of integral equations for the calculation of the band structure and reflectance of one- and two-dimensional photonic crystals," *J. Opt. Soc. Am. B* **23**(10), 2249–2256 (2006).
- ¹³F. Lopes-Tejeira, R. Paniagua-Dominguez, R. Rodríguez-Oliveros, and J. A. Sanchez-Jil, "Fano-like interference of plasmon resonances at a single rod-shaped nanoantenna," *New J. Phys.* **14**, 023035 (2012).
- ¹⁴B. Luk'yanchuk, N. I. Zheludev, S. A. Maier, N. J. Halas, P. Nordlander, H. Giessen, and C. T. Chong, "The Fano resonance in plasmonic nanostructures and metamaterials," *Nat. Materials* **9**, 707–715, (2010).
- ¹⁵H. Lochbihler, "Enhanced transmission of TE polarized light through wire gratings," *Phys. Rev. B* **79**(24), 245427–8 (2009).
- ¹⁶R. Gomez-Medina, M. Laroche, J. J. Saenz, "Extraordinary optical reflection from sub-wavelength cylinder arrays," *Opt. Exp.* **14**(9), 3730–3737 (2006).
- ¹⁷V. O. Byelobrov, J. Ctyroky, T. M. Benson, R. Sauleau, A. Altintas, and A. I. Nosich, "Low-threshold lasing eigenmodes of an infinite periodic chain of quantum wires," *Opt. Lett.* **35**(21), 3634–3636 (2010).
- ¹⁸V. O. Byelobrov, T. M. Benson, and A. I. Nosich, "Near and far fields of high-quality resonances of an infinite grating of sub-wavelength wires," in *Proc. European Conf. Microwaves (EuMC-11)*, Manchester, 858–861 (2011).
- ¹⁹D. M. Natarov, V. O. Byelobrov, R. Sauleau, T. M. Benson, and A. I. Nosich, "Periodicity-induced effects in the scattering and absorption of light by infinite and finite gratings of circular silver nanowires," *Opt. Exp.* **19**(22), 22176–22190 (2011).
- ²⁰T. L. Zinenko, A. I. Nosich, and Y. Okuno, "Plane wave scattering and absorption by resistive-strip and dielectric-strip periodic gratings," *IEEE Trans. Antennas Propag.* **46**, 1498–1505 (1998). [Note that, in the H-case, narrow grating resonances were missing in that paper because of too coarse grid of computation points, in frequency.]
- ²¹T. L. Zinenko and A. I. Nosich, "Plane wave scattering and absorption by flat gratings of impedance strips," *IEEE Trans. Antennas Propag.* **54**(7), 2088–2095 (2006).
- ²²T. L. Zinenko, M. Marciniak, and A. I. Nosich, "Accurate analysis of light scattering and absorption by an infinite flat grating of thin silver nanostrips in free space using the method of analytical regularization," *IEEE J. Selected Topics in Quantum Electronics* **19**(3), DOI:10.1109/JSTQE.2012.2227685 (2013).
- ²³J. R. Krenn, G. Schider, W. Rechberger, B. Lamprecht, A. Leitner, *et al.*, "Design of multipolar plasmon excitations in silver nanoparticles," *App. Phys. Lett.* **77**, 3379–3381 (2000).
- ²⁴O. L. Muskens, V. Giannini, J. A. Sánchez-Gil, and J. Gómez Rivas, "Optical scattering resonances of single and coupled dimer plasmonic nanoantennas," *Opt Exp.* **15**(26), 17736–17746 (2007).
- ²⁵P. Ghenuche, S. Cherukulappurath, T. H. Taminiau, N. F. van Hulst, and R. Quidant "Spectroscopic mode mapping of resonant plasmon nanoantennas," *Phys. Rev. Lett.* **101**, 116805 (2008).
- ²⁶L. J. Anderson, C. M. Payne, Y. R. Zhen, P. Nordlander, and J. A. Hafner, "A tunable plasmon resonance in gold nanobelts," *Nano Lett.* **11**(11), 5034 (2011).
- ²⁷R. A. Depine and D. C. Skigin, "Scattering from metallic surfaces having a finite number of rectangular grooves," *J. Opt. Soc. Am. A* **11**, 2844–2850 (1994).
- ²⁸K. M. Mitzner, "Effective boundary conditions for reflection and transmission by an absorbing shell of arbitrary shape," *IEEE Trans. Antennas Propag.* **16**, 706–712 (1968).
- ²⁹G. A. Grinberg, "Boundary conditions for the electromagnetic field in the presence of thin metallic shells," *Radio Engineering and Electronics* **26**(12), 2493–2499 (1981).
- ³⁰E. Bleszynski, M. Bleszynski, and T. Jaroszewicz, "Surface-integral equations for electromagnetic scattering from impenetrable and penetrable sheets," *IEEE Antennas Propag. Mag.* **35**, 14–25 (1993).
- ³¹J. P. Kottmann and O. J. F. Martin, "Accurate solution of the volume integral equation for high permittivity scatterers," *IEEE Trans. Antennas Propag.* **48**, 1719–1726 (2000).
- ³²J. P. Kottmann and O. J. F. Martin, "Plasmon resonances of silver nanowires with a non-regular cross section," *Phys. Rev. B* **64**(23), 235402–10 (2001).
- ³³O. V. Shapoval, R. Sauleau, and A. I. Nosich, "Scattering and absorption of waves by flat material strips analyzed using generalized boundary conditions and Nystrom-type algorithm," *IEEE Trans. Antennas Propag.* **59**(9), 3339–3346 (2011).
- ³⁴V. Delgado and R. Marques, "Surface impedance model for extraordinary transmission in 1D metallic and dielectric screens," *Opt. Exp.* **19**(25), 25290–25297 (2011).
- ³⁵Q. Cao and P. Lalanne, "Negative role of surface plasmons in the transmission of metallic gratings with very narrow slits," *Phys. Rev. Lett.* **88**, 057403–4 (2002).
- ³⁶H. Lochbihler and R. A. Depine, "Properties of TM resonances on metallic slit gratings," *Appl. Opt.* **51**(11), 1729–1741 (2012).
- ³⁷P. B. Johnson and R. W. Christy, "Optical constants of the noble metals," *Phys. Rev. B* **6**, 4370–4379 (1972).